Medium-Range Forecast Errors Associated with Active Episodes of the Madden–Julian Oscillation

HARRY H. HENDON, BRANT LIEBMANN, MATTHEW NEWMAN, AND JOHN D. GLICK

NOAA–CIRES Climate Diagnostics Center, Boulder, Colorado

J. E. SCHEMM

Climate Prediction Center, NCEP/NWS/NOAA, Boulder, Colorado

(Manuscript received 24 July 1998, in final form 21 December 1998)

ABSTRACT

Systematic forecast errors associated with active episodes of the tropical Madden–Julian oscillation (MJO) are examined using five winters of dynamical extended range forecasts from the National Centers for Environmental Prediction reanalysis model. Active episodes of the MJO are identified as those periods when the amplitude of either of the first two empirical orthogonal functions of intraseasonally filtered outgoing longwave radiation, which efficiently capture the MJO, is large. Forecasts initialized during active episodes of the MJO are found not to capture the eastward propagation of the tropical precipitation and circulation anomalies associated with the MJO. Rather, the MJO-induced anomalies of precipitation and winds are systematically forecast to weaken and even retrograde. By about day 7 of the forecast the convectively coupled, tropical circulation anomalies produced by the MJO are largely gone. Systematic errors in the extratropical 200-mb streamfunction also fully develop by day 10. The initial development of these errors is argued to result from the collapse of the tropical divergence forcing produced by the MJO and, thus, the lack of correct Rossby wave source. Forecast skill in the Tropics and Northern Hemisphere extratropics is found to be systematically reduced during active periods of the MJO as compared to quiescent times. This reduced skill is suggested to result because the MJO is the dominant mode of convective variability and not because the model is better able to forecast intraseasonal convection unrelated to the MJO.

1. Introduction

The Madden–Julian oscillation (MJO) is the dominant mode of intraseasonal variability and covariability of convection and circulation in the Tropics (e.g., Zhang and Hendon 1997). The variability and coupling of convection and circulation produced by the MJO is strongest across the eastern Indian and western Pacific Oceans (e.g., Salby and Hendon 1994), where there is significant impact on the climate of this region. For instance, the MJO has been linked to the onset and variability of the Australian monsoon (e.g., Hendon and Liebmann 1990), modulation of tropical cyclone development (Nakazawa 1986; Liebmann et al. 1994), and intraseasonal variations of sea surface temperature across the warm pool (e.g., Zhang 1996; Hendon and Glick 1997) that may be important for the onset of some El Niño events (Kessler et al. 1995).

Although the influence of the MJO on the extratropics is less robust than in the Tropics, significant global-scale circulation anomalies evolve in concert with the life cycle of the tropical convective anomalies (e.g., Lau and Phillips 1986; Knutson and Weickmann 1987). These global-scale circulation anomalies have been interpreted to involve not only a directly forced component by the tropical convective anomalies associated with the MJO but also to result from the internal dynamics of the extratropical circulation (e.g., Simmons et al. 1983; Lau and Phillips 1986; Ferranti et al. 1990; Hsu 1996).

The intraseasonal timescale of the circulation and convective anomalies produced by the MJO suggests the potential for significant impact on medium- and extended-range (i.e., beyond one week) forecasts, particularly during boreal winter when the MJO is most active (e.g., Salby and Hendon 1994). Such impact would extend not only to the Tropics, where extended-range prediction of monsoon onset or tropical cyclone development may be of considerable value, but also to the extratropics. For instance, extratropical circulation anomalies develop across the North Pacific about one week after the eastward shift of anomalous convection as-

Corresponding author address: Harry Hendon, Climate Diagnostics Center, Mail Code R/CDC1, 325 Broadway, Boulder, CO 80303-3328.
E-mail: hhh@cdc.noaa.gov

sociated with the MJO into the western tropical Pacific (Higgins and Mo 1997). Other studies have found that extended-range forecasts skill in the extratropics is significantly impacted by the presence of strong MJO activity (e.g., Ferranti et al. 1990). Together, these results suggest that proper simulation of the tropical MJO could lead to substantial improvement of global medium- and extended-range forecasts, especially during the one or two significant MJO events each boreal winter (e.g., Salby and Hendon 1994).

The present study extends earlier work by examining systematic errors associated with active episodes of the MJO using 5 yr of dynamical extended-range forecasts. At the onset, little skill in predicting the evolution of the MJO is anticipated because global forecast models run as climate models do not simulate the MJO well (e.g., Slingo et al. 1996), presumably due to problems with the convective parameterizations or the neglect of ocean–atmosphere coupling on these timescales (e.g., Wang and Xie 1998). Furthermore, large errors are present in the initial tropical analyses. These errors are due both to a paucity of observations and the lack of direct observations and assimilation of divergence and diabatic heating, which are fundamental components of the MJO. For instance, Shinoda et al. (1999) have shown that intraseasonal rainfall variance across the warm pool, where the MJO is most pronounced, is about a factor of 4 weaker in the National Centers for Environmental Prediction (NCEP) reanalyses (which are used as the initial conditions for the forecast model in this study and also reflect the model's convective parameterization; Kalnay et a1. 1996) than from satellite observations. This combination of problematic model physics and initial condition errors makes dynamical prediction of the MJO in a global forecast model a daunting task. Hence, this study will emphasize the development of systematic forecast error in the Tropics during active episodes of the MJO and the subsequent development of systematic extratropical error and its relation to tropical divergence forecast error.

2. Data and analysis procedure

The forecast data come from a series of dynamic extended-range forecasts from January 1985 through March 1990 (Schemm et al. 1996). The forecast model is the T62L28 reanalysis version of the NCEP medium-range forecast (MRF) model (Kalnay et al. 1996). Fifty-day forecasts were initialized each day using the OZ reanalysis as initial conditions. During the forecast, sea surface temperature was damped to climatology from the observed initial condition with a 90-day *e*-folding time, which may adversely affect prediction of the MJO. The present study utilizes forecasts through day 15 of precipitation and the winds at 200 and 850 mb. The NCEP reanalysis is used as the verification. All analyses are performed on data that have been truncated to T12 (unless otherwise indicated), which emphasizes the large-scale anomalies produced by the MJO. The global aspect of the MJO circulation anomalies and associated forecast errors are primarily examined using the 200-mb streamfunction (generated from the 200-mb wind field).

The observed level of MJO convective activity is quantified using empirical orthogonal function (EOF) analysis, performed on unnormalized, intraseasonally filtered outgoing longwave radiation (OLR) in the domain 30°N–30°S for 1979–94. EOF analysis of intraseasonally filtered OLR efficiently extracts the dominant mode of eastward propagating convection associated with the MJO (e.g., Ferranti et al. 1990; Zhang and Hendon 1997). EOF analyses of velocity potential have also been used to isolate the MJO (e.g., Lorenc 1984). However, because velocity potential is not a local measure of divergence (e.g., Hendon 1986), use of OLR is preferable in this study, as it more directly captures localized convective heating anomalies produced by the MJO.

Details of the OLR data are provided by Liebmann and Smith (1996). Intraseasonal filtering was accomplished by Fourier spectral transform, with periods between 26 and 100 days retained (full power at 26 and 100 days, half-power at 25 and 110 days, and zero power at 24 and 120 days). Prior to performing the EOF analysis, the filtered OLR was averaged onto a 5° lat by 10° long grid.

The first two EOFs of intraseasonally filtered OLR, which together account for about 21% of the filtered variance, describe an eastward propagating convective disturbance with an approximate 45-day period. The eigenvectors (not shown, but see, e.g., Ferranti et al. 1990) depict variability with a local zonal wavenumber 2 structure, concentrated across the equatorial Indian and western Pacific Oceans and extending eastward into convergence zones of the central Pacific.

We define strong MJO activity as occurring whenever either of the two leading principal components exceeds 1.5 standard deviations during the 5-yr period for which the forecasts are available.[1] Four phases during the life cycle of the MJO are then signified as PC1+, PC2+, PC1−, and PC2−. Each succeeding phase typically leads the preceding phase by ¼ cycle (about 12 days), with anomalies during plus phases being generally opposite to those during minus phases. Table 1 displays the dates of maximum excursion for each phase. Since all dates are between November and March, all subsequent analyses will be confined to that extended winter season.

For compositing purposes, dates up to 5 days on either side of these maxima are included as long as the amplitude of the principal component remains at least 1

[1] Note that a 1.5 standard deviation excursion using the entire 16-yr record is roughly equivalent to a 1 standard deviation excursion if only November–March is considered.

TABLE 1. Dates of maximum excursion (exceeding at least 1.5 standard deviations) of the first two principal components of intraseasonally filtered OLR. The range of days for which the principal component remains at least 1 standard deviation, up to 5 days on either side of the maximum, is listed in parentheses. The right-hand column (labeled ''quiescent'') lists the range of days when both principal components are simultaneously less than 0.5 standard deviation.

	PC1+	PC2+	PC1−	PC2−	Quiescent
1	5 Feb 1985 (−5, +5)	16 Feb 1985 (−5, +5)	26 Feb 1985 (−5, +5)	22 Jan 1985 (−5, +4)	29–30 Mar 1995
2	3 Jan 1986 (−5, +5)	16 Jan 1986 (−5, +5)	14 Nov 1986 (−5, +5)	5 Feb 1986 (−4, +4)	9–13 Nov 1985
3	12 Mar 1986 (−5, +5)	5 Nov 1986 (−3, +3)	7 Feb 1987 (−4, +5)	24 Dec 1986 (−5, +4)	Nov–10 Dec 1985
4	2 Nov 1987 (−3, +2)	16 Jan 1987 (−3, +3)	19 Nov 1987 (−4, +4)	1 Jan 1988 (−4, +5)	22–28 Feb 1986
5	5 Dec 1987 (−5, +5)	7 Feb 1988 (−5, +5)	22 Dec 1987 (−4, +3)	2 Mar 1988 (−5, +5)	Nov–5 Dec 1986
6	24 Jan 1988 (−5, +5)	24 Mar 1988 (−5, +5)	14 Feb 1988 (−5, +5)		21–26 Mar 1987
7	13 Jan 1989 (−5, +5)		20 Dec 1988 (−5, +5)		26–29 Nov 1987
8					1–14 Nov 1988
9					10–19 Feb 1989
Total days	72	58	71	50	62

standard deviation (Table 1). Inclusion of these extra dates not only removes some of the noise from the observed composite but also is an attempt to incorporate an ensemble of initial conditions for forecasts of each of the four phases of the MJO. For each of the four phases there are between 5 and 7 events, which include between 50 and 72 individual forecasts. Also included in Table 1 are the dates of null projection onto the leading two principal components during November–March. These dates are determined whenever the amplitudes of both principal components are simultaneously less than 0.5 standard deviation. These 62 null days will be used to determine skill for forecasts initialized during ''quiescent'' episodes of the MJO.

Composites of forecasts for each of the four phases of the MJO (as well as for the quiescent times) are made in two ways. The first is to composite the forecasts, as a function of forecast lead time, that all are *initialized* at the maxima of the OLR PCs (i.e., initialized on the dates listed in Table 1). This method reveals the ability to forecast the evolution of the MJO once the MJO already has significant amplitude. The second method is to composite forecasts with the same lead times but that all *verify* on the maxima of the OLR PCs. This method emphasizes the ability to forecast the development of the MJO. In this latter method, composites for each different lead time are formed from forecasts that begin from different initial conditions.

3. Mean model error

Prior to forming composites of the systematic forecast errors during each phase of the MJO, the mean model error is diagnosed and removed. Its removal helps distinguish the error associated with each phase of the MJO. An important assumption is made here that the mean model error is independent of the MJO and thus can be linearly removed. Comparison of error fields during active MJO and quiescent MJO periods suggests this to be the case. The mean model error, as a function of forecast lead time, is determined by forming the composite daily annual cycle of the difference between the forecasts and the verifying analysis. This composite daily difference at each lead time is harmonically filtered, retaining the mean and first three annual harmonics, and then removed from all forecasts prior to subsequent analysis.

Figure 1 displays the five-winter mean (November–March) eddy 200-mb streamfunction and mean model error at forecast lead time 15 days. The mean model error has about one-half the magnitude of the eddy stationary waves and represents a general weakening of them (note that the contour interval for the mean error is one-half that of the analysis). Consistent with the analysis by Cai et al. (1996) of a similar version of the MRF model, an easterly bias develops in the tropical upper troposphere and the midlatitude jets are displaced poleward (not shown).

The five-winter mean eddy 850-mb zonal wind and 200-mb divergence for the tropical Indian and western Pacific Oceans are shown in Fig. 2. This monsoon region is of particular relevance to this study, as it is where the MJO exhibits its largest amplitude. In the African and Indonesian monsoons, lower-tropospheric westerlies coincide with regions of enhanced precipitation (Fig. 1a) and upper-tropospheric divergence (Fig. 2). The region of strong divergence to the east of the Philippines is a noteworthy exception. However, the analyzed divergence (and precipitation) is probably in error for this region (Newman et al. 2000). The mean model error for the 200-mb divergence (not shown) reveals a weakening of the divergent outflow associated with con-

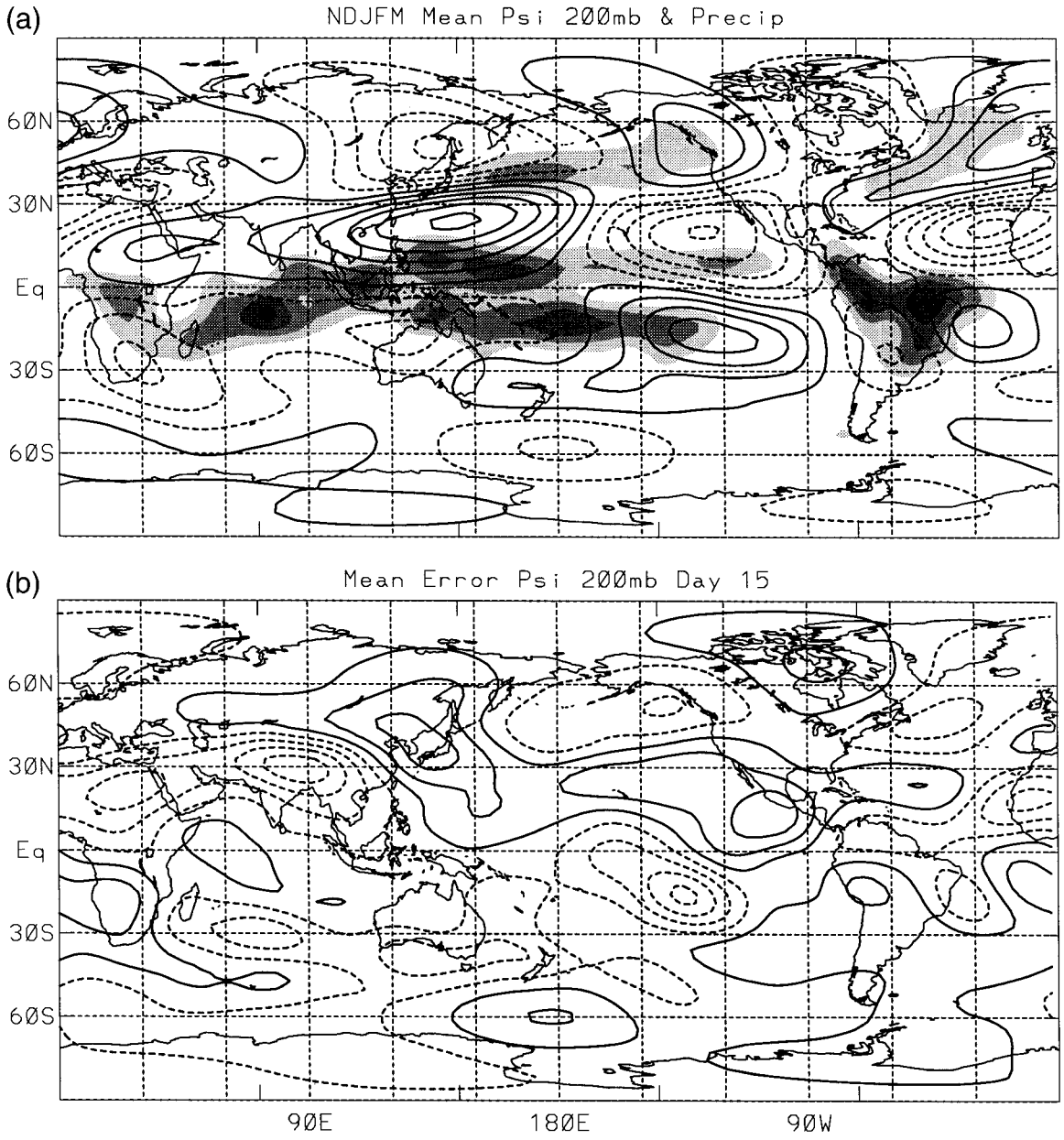

FIG. 1. (a) Nov–Mar mean 200-mb eddy streamfunction and precipitation from the NCEP reanalysis. The contour interval for streamfunction is 5×10^6 m^2 s^{-1} (negative values dashed), with the first contour at $\pm 2.5 \times 10^6$ m^2 s^{-1}. The shading level for precipitation is 2 mm day^{-1} with the first level at 4 mm day^{-1}. (b) Five-winter mean model error for the 15-day forecast of 200-mb streamfunction. Contour interval is 2.5×10^{-6} m^2 s^{-1} with first contour at $\pm 1.25 \times 10^6$ m^2 s^{-1}.

vection over the ''maritime continent,'' over the south equatorial Indian Ocean, and in the South Pacific convergence zone of the western Pacific. Erroneous upper-level outflow (and convection) occurs along the equator in the western Pacific and north of the equator in the western Indian Ocean. The relationship between erroneous upper-level divergence and lower-level zonal wind is complicated but generally indicative of thermally direct, deep forcing (i.e., erroneous upper-tropospheric outflow is associated with erroneous precipitation and lower-tropospheric inflow).

The development of these errors is shown in Fig. 3, which displays the mean model error for the eddy 850-mb zonal wind and precipitation averaged from 5°N to 15°S as a function of forecast lead time. For both precipitation and zonal wind, the error grows rapidly for the first 7–10 days and then appears to saturate. Similar saturation occurs for the 200-mb eddy streamfunction

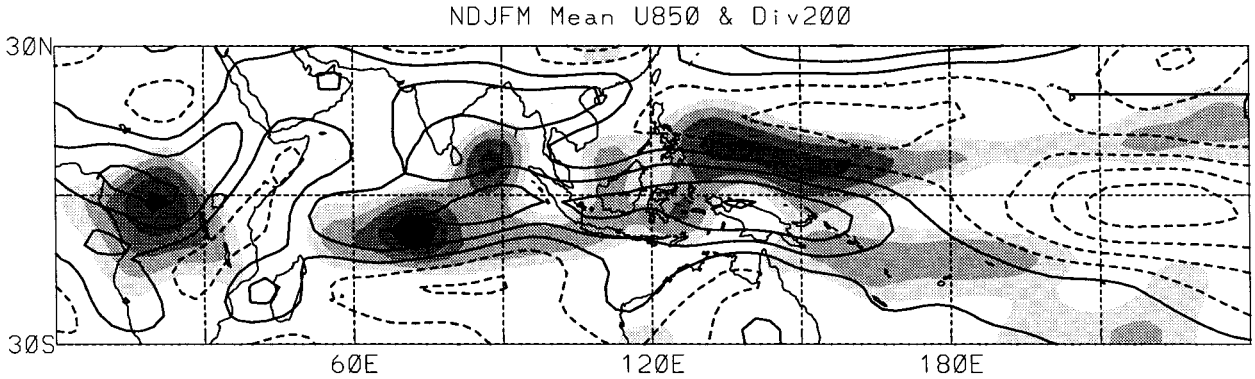

FIG. 2. Five-winter mean eddy zonal wind at 850 mb and the 200-mb divergence. The contour interval for zonal wind is 2 m s^{-1}, with first contour at ± 1 m s^{-1}. The shading level for divergence is 1×10^6 s^{-1}.

error (not shown). Note also that the magnitude of the mean precipitation errors by day 10 are also about one-half that of the mean precipitation in this equatorial band (Fig. 1a). In contrast to the behavior of the MJO, the mean model error in the Tropics develops in place with little indication of zonal propagation. This suggests the mean model error is not simply the systematic misrepresentation of the MJO.

4. Observed MJO

Before examining forecast skill during active episodes of the MJO, composite observations of the MJO, based on the dates listed in Table 1, are reviewed. Prior to forming the composites, anomalies are formed by removing the annual cycle of the analyses (the mean and three annual harmonics of the composite seasonal cycle). Otherwise, no other filter is applied.

Figure 4 shows the composite eddy 850-mb zonal wind (zonal mean removed to emphasize zonal variations relative to the convective anomalies) and OLR anomalies for the PC1+ and PC2+ phases. Composite anomalies for PC1− and PC2− (not shown) generally have the same structure as PC1+ and PC2+, respectively, but with opposite sign. Composites of the global eddy 200-mb streamfunction and divergence anomalies are displayed in Fig. 5. The 95% significance level for the streamfunction anomalies is indicated by cross hatching. Significance was determined by comparing the composite anomalies to the standard deviation of 5-day running mean streamfunction, using a two-sided *t* test and assuming one degree of freedom for every 5 days of analyses included in each phase of the composite. Significance, so defined, occurs when the composite anomalies exceed approximately one-half the local standard deviation of the 5-day running mean streamfunction. Significance for the other fields displayed in Figs. 4 and 5 are not indicated, but is implied, at least in the Tropics, wherever their magnitudes exceed about one contour level.

The sequence of anomalies displayed in Figs. 4 and 5 is typical of the life cycle of the MJO: equatorial convection and associated upper-tropospheric divergence display a local zonal wavenumber 2 structure across the Indian and western Pacific Oceans and propagate eastward at about 5 m s^{-1}. Lower-tropospheric, near-equatorial westerlies occur west of the anomalous convection, with easterlies to the east. At upper levels, subtropical anticyclones straddle and slightly trail anomalous convection, with cyclones straddling and slightly trailing regions of suppressed convection. Note that some of the extratropical anomalies, especially over

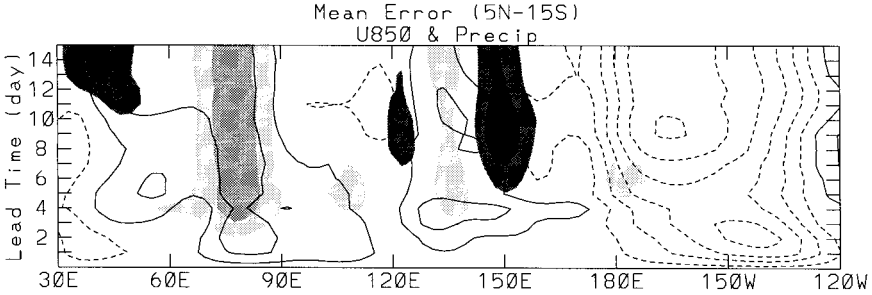

FIG. 3. Five-winter mean model error, as a function of forecast lead time, for the eddy 850-mb zonal wind and precipitation, averaged between 5°N and 15°S. The contour interval for zonal wind is 0.5 m s^{-1}, with first contour at ± 0.25 m s^{-1}. Shading level for precipitation is 1 mm day^{-1} (darker shades are positive errors).

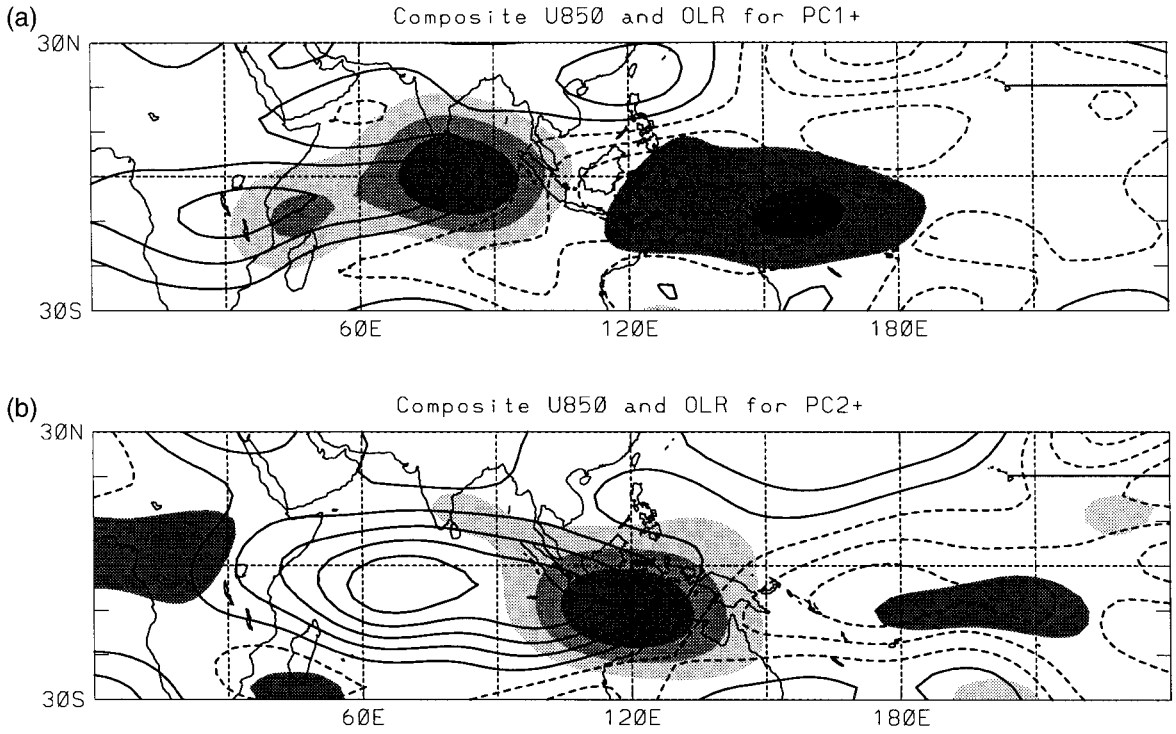

FIG. 4. Composite anomalies (annual cycle removed) of eddy zonal wind at 850 mb and OLR for times of maximum (a) PC1+ and (b) PC2+. Contour interval for zonal wind is 1 m s^{-1} (first contour ± 0.5 m s^{-1}). Shading level for OLR is 10 W m^{-2} (darker shades are positive anomalies).

the higher latitudes of Asia and North America, are only marginally significant, although their structure is typical of previous composite analyses of the MJO (e.g., Knutson and Weickmann 1987).

The implied evolution of the extratropical streamfunction anomalies depicted in Fig. 5 also agrees well with previous studies of the life cycle of the MJO (e.g., Knutson and Weickmann 1987; Hsu 1996). Prominent features include a weakening and contraction of the East Asian jet as the convective anomaly develops in the Indian Ocean and moves eastward toward Indonesia (phases PC1+ and PC2+) and a similar strengthening and expansion of the jet during the other two phases. The evolution of the extratropical anomalies has both the appearance of simple Rossby wave dispersion from a tropical source (e.g., the wave trains arcing across the South Pacific for the PC1+ phase), and in situ extratropical development (e.g., the development of the extratropical anomalies in the Northern Hemisphere in going from phase PC1− to PC2−). Such behavior, however, is consistent with the notion that the extratropical circulation anomalies are the result of a Rossby wave source, associated with anomalous tropical convection, acting in a wavy basic state (e.g., Sardeshmukh and Hoskins 1988; Ferranti et al. 1990; Hsu 1996).

5. Systematic MJO error

Systematic forecast error associated with MJO is first explored by considering forecasts *initialized* during active phases of the MJO, as defined by the dates in Table 1. Figures 6 and 7 display Hovmöller plots of equatorial averaged analyses and forecasts for the 850-mb zonal wind and precipitation, composited relative to times of maximum PC1+ and PC2+. Plots for the other two phases (not shown) are similar, but of opposite sign. The composite analyses, running from 14 days prior to 14 days after the dates listed in Table 1, are shown in the upper panels, while the lower panels display the composite forecasts *intialized* at the time of maximum of the PCs. The analyses depict coherent eastward propagation at about 5 m s^{-1}, which typifies the MJO. In contrast, the composite forecasts exhibit no indication of eastward propagation. Rather, the initial precipitation anomalies tend to remain stationary (and even retrogress) and decay. By about 7 days the MJO is essentially absent from the forecasts.

The development of the tropical error is further illustrated in Fig. 8, which displays composite 850-mb zonal wind and 200-mb divergence errors for the 3-, 7-, and 11-day forecasts that all *verify* at the time of maximum PC1+. The same error pattern, essentially of opposite sign to the composite analysis (see Fig. 4a), emerges for each successively longer lead time, but with magnitude proportional to the length of forecast. A similar evolution holds for the other three phases. These results again indicate that the convectively coupled tropical circulation anomalies produced by the MJO systematically decay to zero by about day 7 of the forecasts.

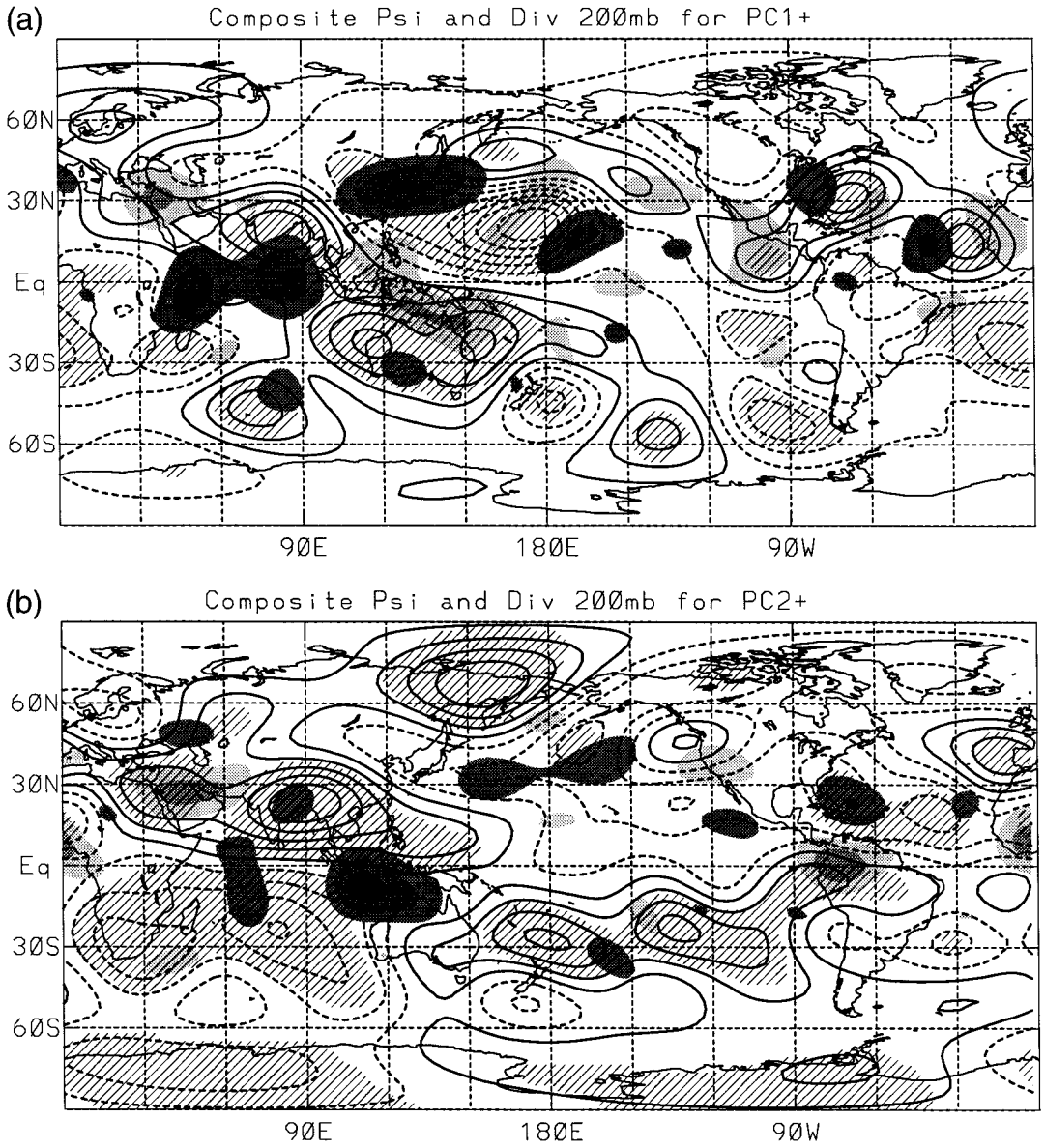

FIG. 5. Composite anomalies (annual cycle removed) of eddy 200-mb streamfunction and divergence for times of maximum (a) PC1+ and (b) PC2+. The contour interval for streamfunction is 2.5×10^{-6} m^2 s^{-1} with first contour at $\pm 1.25 \times 10^6$ m^2 s^{-1}. Shading level for divergence is 1×10^{-6} s^{-1} (darker shades are positive anomalies). Cross hatching indicates 95% significance level for streamfunction anomalies.

The impact on the extratropics of this failure to maintain or properly evolve the convectively coupled components of the MJO in the Tropics is now examined. Composite 200-mb streamfunction and divergence errors are shown in Fig. 9 for the 15-day forecasts verifying on the maximum of PC1+ and PC2+ (i.e., for forecasts *initialized* 15 days prior to the dates shown in Table 1 for PC1+ and PC2+). The errors for each phase generally look like the negative of the verifying composite analyses (i.e., Fig. 5), implying that the error by day 15 is about 100%, regardless of the initial phase of the MJO.

Erroneous tropical divergence due to erroneous precipitation in the Indian and west Pacific Oceans apparently acts to force Rossby wave trains that systematically develop downstream as the duration of the forecast extends. This is illustrated in Fig. 10, which shows the 200-mb streamfunction error for forecasts *verifying* on the maximum of PC1+. The similarity of the 11-day (Fig. 10c) and 15-day (Fig. 9a) forecasts suggests that the extratropical error is fully developed by about 11 days. The development of the forecast error for the other phases (not shown) exhibits more complicated behavior, with evidence of dispersion into the extratropics, as well

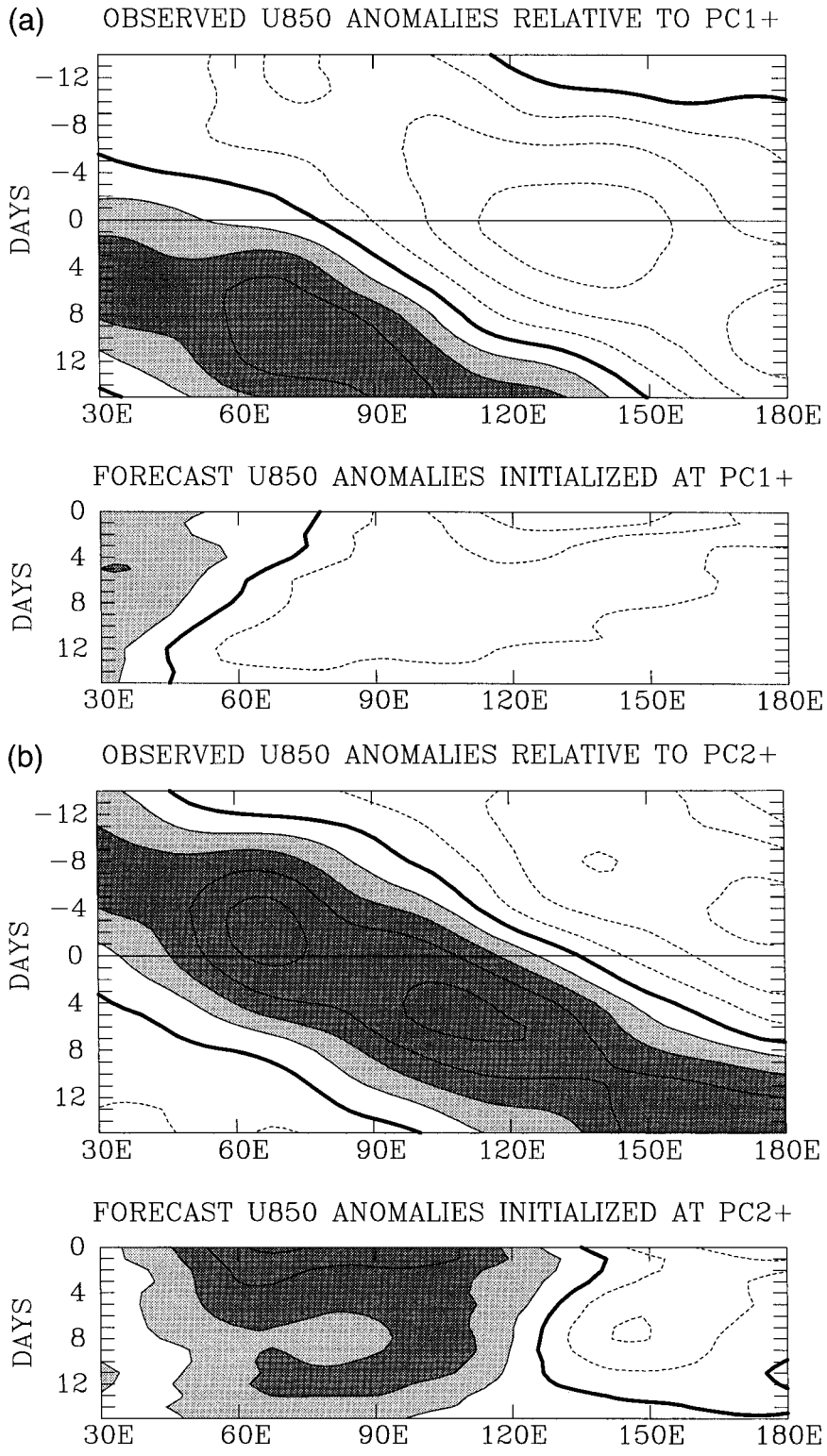

FIG. 6. Composite anomalies (annual cycle removed) of 850-mb zonal wind (contour interval 1 m s^{-1}) relative to (a) maximum PC1+ and (b) maximum PC2+. Anomalies have been averaged from 5°N to 15°S. The upper panels are the observed anomalies from time −14 days to +14 days, where day 0 is the maximum of the PC. The lower panels are forecast anomalies (mean model error and annual cycle removed) initialized at day 0.

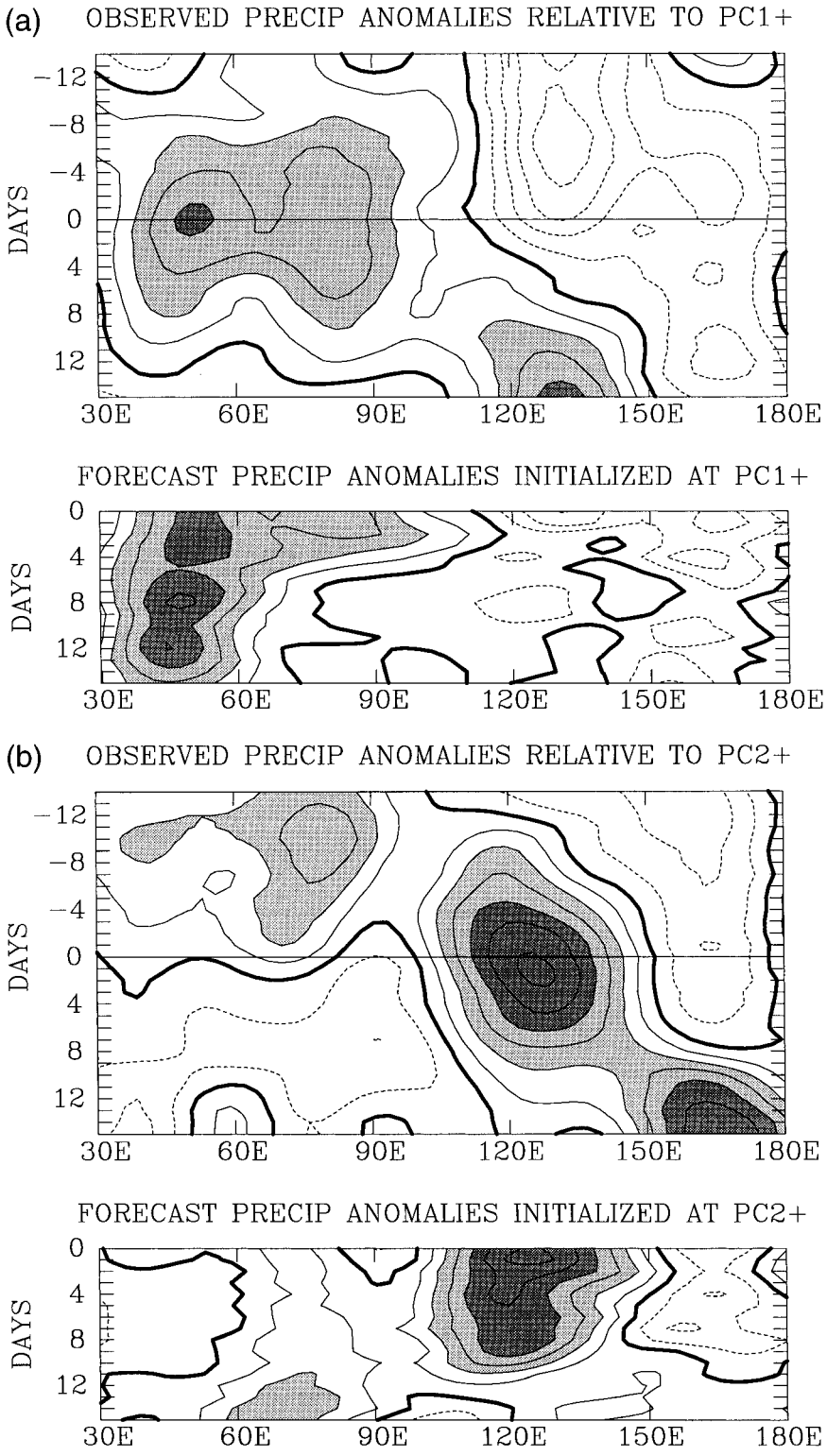

FIG. 7. As in Fig. 6 except for precipitation anomalies (contour interval 1 mm day^{-1}).

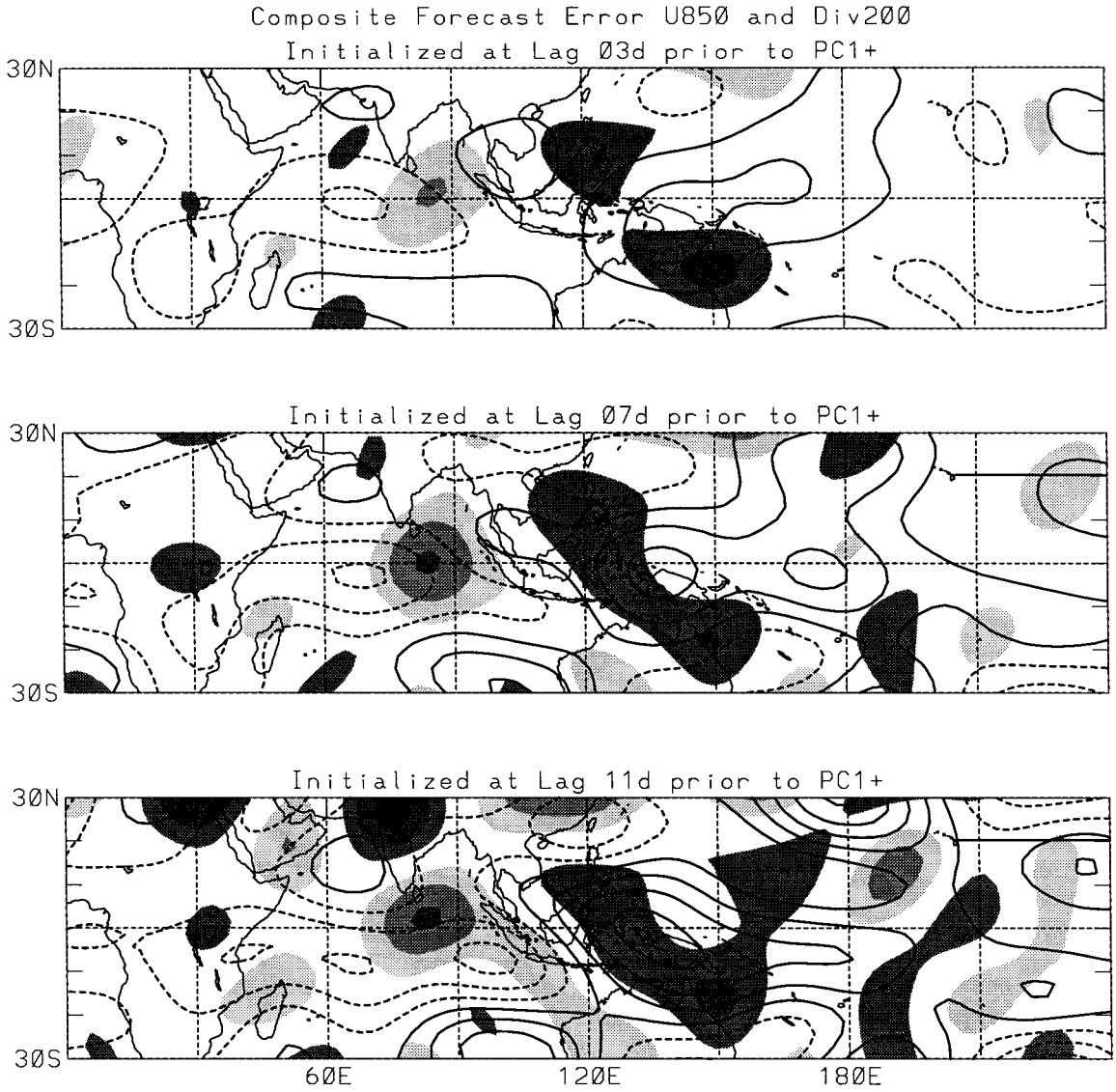

FIG. 8. Composite forecast error (forecast minus observed anomalies) of the eddy 850-mb zonal wind (contoured) and 200-mb divergence (shaded) for (a) the 3-day forecasts, (b) the 7-day forecasts, and (c) the 11-day forecasts that verify at the time of maximum PC1+. The contour interval for zonal wind is 1 m s^{-1}. The shading level for divergence is 1×10^{-6} s^{-1} with darker shades for positive errors.

as apparent in situ development in the extratropics. Such development of the forecast error, however, is consistent with the notion that these extratropical model errors are primarily forced by the collapse of the tropical divergence forcing produced by the MJO (e.g., Fig. 8), but that the details of the associated erroneous Rossby wave source acting in a wavy basic state need to be considered (e.g., Sardeshmukh and Hoskins 1988; Ferranti et al. 1990).

The magnitude of the systematic streamfunction error associated with the failure to predict the evolution of the MJO is comparable to the mean model error and random forecast error (i.e., with the mean model error removed). For example, the typical systematic error associated with active episodes of the MJO can be evaluated by zonally averaging the square root of the four-phase mean-squared composite MJO error of the 200-mb eddy streamfunction (Fig. 11a). This is compared to the zonal mean of the root-mean-square (rms) mean model error (Fig. 11b) and random forecast error (Fig. 11c) for the 200-mb eddy streamfunction (note that the scale of the abscissa is doubled from that in Figs. 11a and 11b). The zonal mean of the 5-day mean standard deviation of the observed eddy streamfunction is also shown in Fig. 11c. Prior to computing the random forecast error, a running 5-day mean was applied to the analyses and forecasts (e.g., the smoothed day 3 forecast consists of the average of the day 1–5 forecasts made from the same initial condition). This 5-day mean was applied to allow for a more direct comparison with the

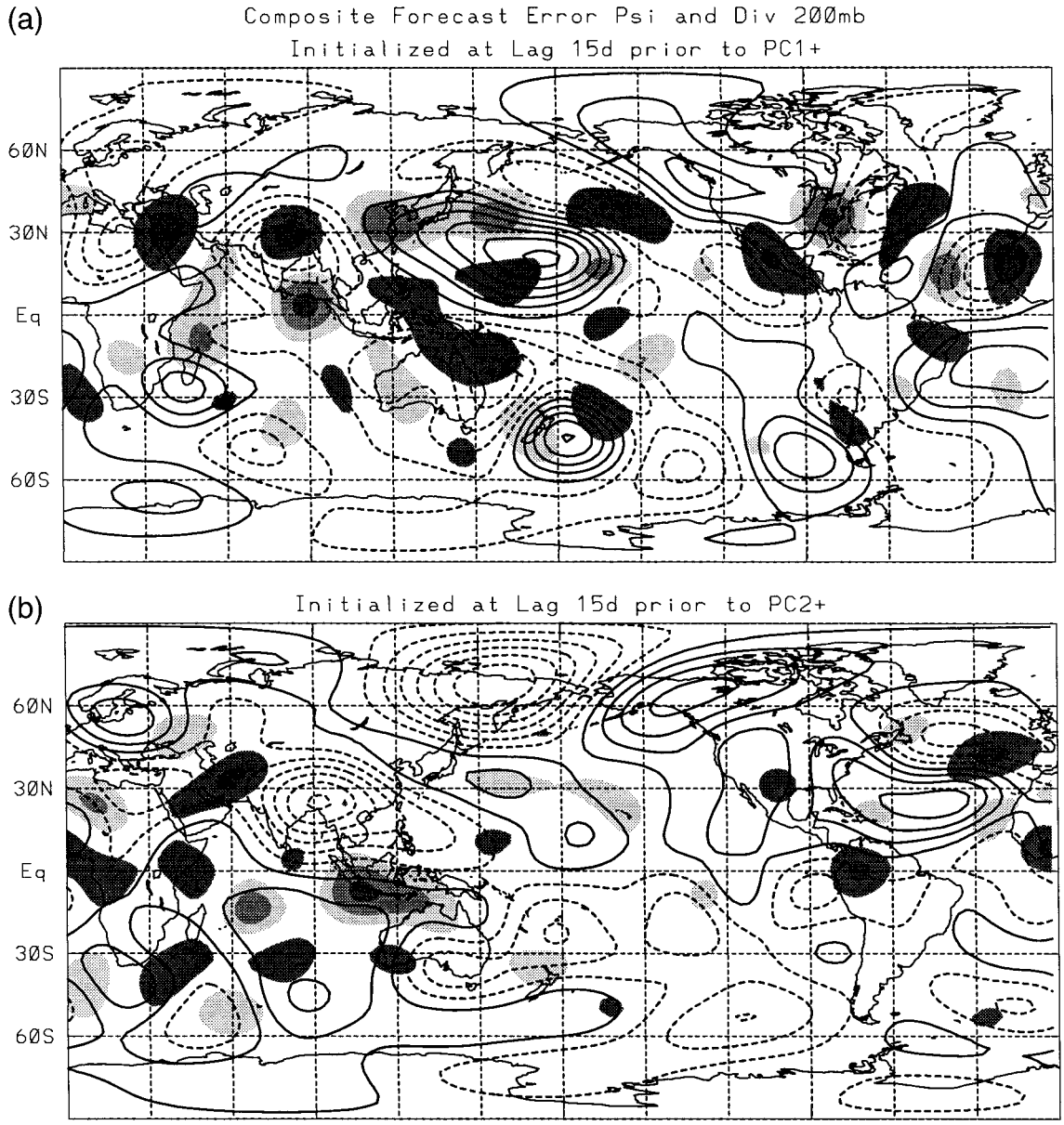

FIG. 9. Composite forecast error of the eddy 200-mb streamfunction (contoured) and divergence (shaded) for the 15-day forecasts that verify at the time of maximum (a) PC1+ and (b) PC2+. Contour and shading intervals are as in Fig. 5.

systematic MJO errors, which have been derived from forecasts that have been effectively low-pass filtered due to the compositing method. The magnitude of the systematic error associated with active periods of the MJO is seen to be comparable to that of the mean model error by day 8 and exceeds it by up to a factor of 2 (particularly in the Southern Hemisphere midlatitudes and poleward of 45°N) by day 13 (cf. also Fig. 1b and Fig. 9). The magnitude of the systematic MJO error is about one-third to one-half of the 5-day mean standard deviation of the analyses and also of the random error by day 13 (Fig. 11c).

Another way to quantify the systematic MJO error is to examine anomaly correlations and rms difference between forecast and verification as functions of forecast lead time. Anomaly correlations and rms differences were computed using 5-day mean analyses and forecasts. The mean model error was first removed and anomalies were formed for both analyses and forecasts by removing the annual cycle. Correlations and rms differences were formed for all spatial points in specified domains (weighted by the cosine of latitude) and over all forecasts *initialized* when the MJO was active (all dates in the first four columns of Table 1). Anomaly correlations were also computed over all forecasts *initialized* when the MJO was quiescent (column 5 in Table

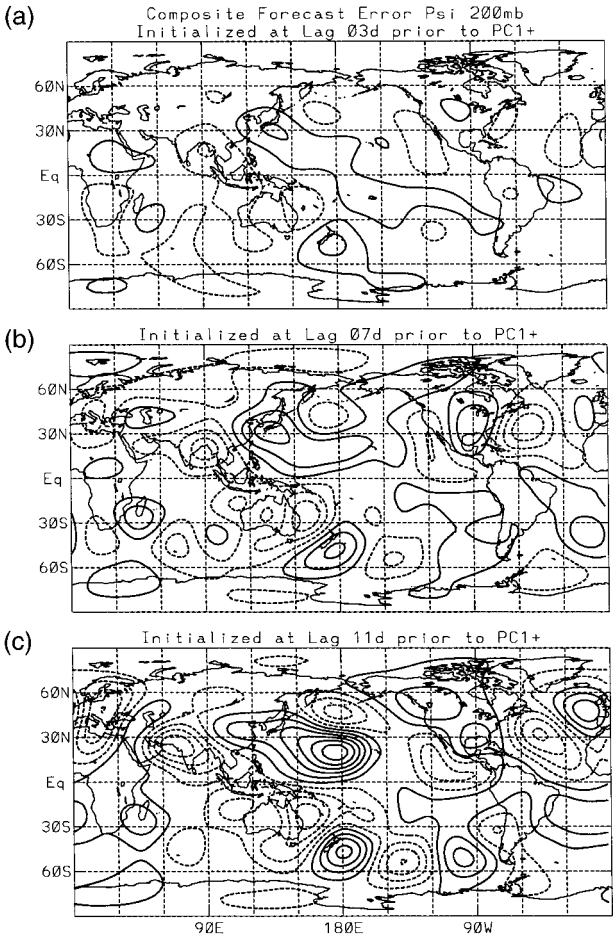

FIG. 10. Composite forecast error of the eddy 200-mb streamfunction for the (a) 3-day, (b) 7-day, and (c) 11-day forecasts that verify at the time of maximum PC1+. Contour intervals are as in Fig. 5.

1), and when the MJO was ''nonactive'' (i.e., for all available November–March dates except those listed in the first four columns of Table 1, which number about 500 individual forecasts).

Figure 12a displays the anomaly correlations of the 200-mb eddy streamfunction for the tropical region (30°N–30°S, 30°E–120°W), where the 200-mb cyclone–anticyclone couplet produced by the MJO is most pronounced (e.g., Fig. 4). Anomaly correlations in the region of largest response in the Northern Hemisphere extratropics (30°–90°N, 90°E–90°W) are shown in Fig. 12b. The entire Southern Hemisphere extratropics (30°–90°S) are included in Fig. 12c, as little longitudinal dependence of the impact is found there. Similar plots of the rms forecast error, normalized by the rms of the verification, are shown in Fig. 13. In the Tropics and Northern Hemisphere extratropics, after about day 4, skill for the quiescent periods is systematically best followed by nonactive periods and finally active periods. On the other hand, forecasts initialized when the MJO is active do seem to be better in the Southern Hemisphere extratropics, where the quiescent and nonactive periods are systematically worse than the active cases after about day 4.

Also shown in Figs. 12a and 13a are anomaly correlations for the canonical MJO, formed by lag regression of the observed streamfunction anomalies onto the leading two PCs of OLR at the initial forecast time. The explained variance by the canonical MJO is initially much less than for the model forecasts in the Tropics (Fig. 12a), as would be expected because information about the random initial conditions is ignored. But, by day 7 when the MJO anomalies are effectively gone from the model forecasts, the canonical MJO anomalies explain more variance than the model forecasts. By day 13, the canonical MJO accounts for about 25% of the spatial variance in the Tropics, while the model forecasts account for less than 10%.

These results suggest that further forecast improvement is possible by removing the systematic MJO error (as a function of forecast lead time) from those forecasts initialized during active episodes of the MJO. The systematic MJO error, as a function of forecast lead time, was determined by lag regression of the forecast error (after removing the mean model error) onto the leading two principal components of OLR at the initial time.[2] The spatial distribution of this regressed error (not shown) is similar to the composite error (e.g., Fig. 9), and thus is similar to the negative of the canonical MJO anomalies. The impact of this empirical correction on the forecasts initialized when the MJO is active is uniformly positive, with an impressive increase of the tropical anomaly correlation from 0.23 to 0.45 and a 10% decrease of the rms error at day 13.[3] Less improvement occurs in the extratropics (e.g., the day 13 correlation increases from 0.31 to 0.36 in the Northern Hemisphere extratropics, and from 0.19 to 0.26 in the Southern Hemisphere extratropics), which is consistent with the fact that the MJO signal is weaker in the extratropics than in the Tropics. Correcting forecasts initialized during nonactive periods produced minimal improvement in skill.

6. Barotropic simulations

The reanalysis version of the MRF model can neither sustain the eastward propagating tropical components of the MJO when initialized at times the MJO is active

[2] A ''forecast'' of the state of the MJO at the verifying time is apparently made by this technique. That is, the error of a 15-day forecast is predicted by the regression based on the state of the MJO 15 days prior. However, it is interesting to note that correcting the forecasts with the error regressed onto the principal components at the verifying time does not lead to any further improvement, presumably because the full development of the systematic MJO error takes at least 10 days.

[3] It is important to emphasize that more modest improvements would be expected in an operational setting because here the forecasts that are corrected are included in the regression analysis.

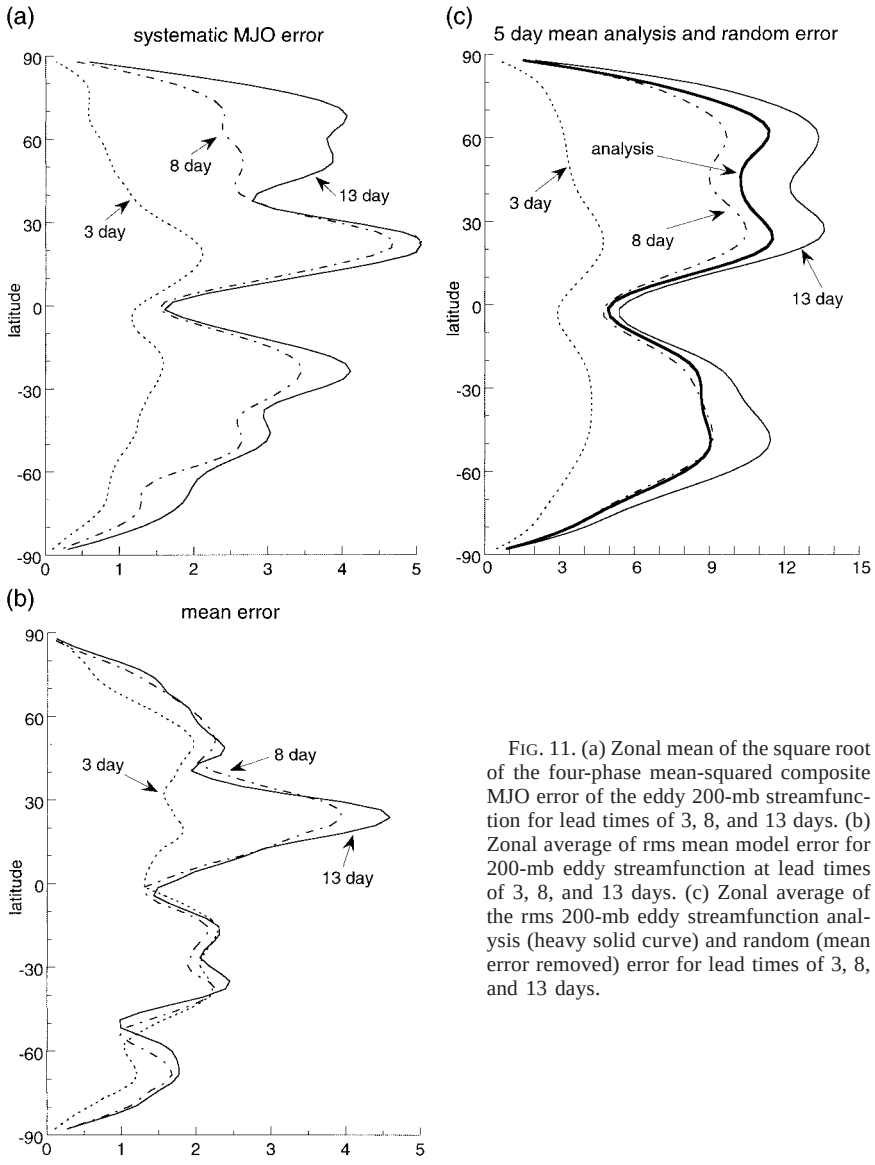

FIG. 11. (a) Zonal mean of the square root of the four-phase mean-squared composite MJO error of the eddy 200-mb streamfunction for lead times of 3, 8, and 13 days. (b) Zonal average of rms mean model error for 200-mb eddy streamfunction at lead times of 3, 8, and 13 days. (c) Zonal average of the rms 200-mb eddy streamfunction analysis (heavy solid curve) and random (mean error removed) error for lead times of 3, 8, and 13 days.

nor develop an active MJO when initialized prior to such observed development. Systematic forecast errors of the extratropical circulation subsequently develop and are well established by about day 7 into the forecast. By about day 11, when the MJO has essentially decayed to zero in the forecasts, the systematic extratropical error is about 100% of the observed MJO anomalies.

These systematic extratropical errors appear, at least initially, to be due to the collapse of the tropical divergence forcing produced by the MJO and, thus, the lack of the Rossby wave source as the MJO evolves. To test this hypothesis, we consider the evolution of the 200-mb streamfunction error in a linear barotropic vorticity model [e.g., Sardeshmukh and Hoskins 1988; their Eq. (6)] forced by the forecasts divergence errors. The model is linearized about the observed five-winter mean rotational and divergent wind at 200 mb.[4] To emphasize the role of the erroneous tropical divergence, the systematic MJO divergent wind errors are windowed in latitude to include only the Tropics. The model is integrated by expanding all variables in a series of spherical harmonics, truncated at T42, and by linearly interpolating the daily composite divergent wind errors to the model time step of 0.5 h. Linear damping is included with a timescale of 7 days. Such a damping timescale

[4] The barotropic model was also linearized about the five-winter average 200-mb flow minus the MRF mean error, as a function of forecast lead time, in order to investigate the impact of error in the basic state of the MRF on the evolution of the extratropical streamfunction errors. No significant impacts were found.

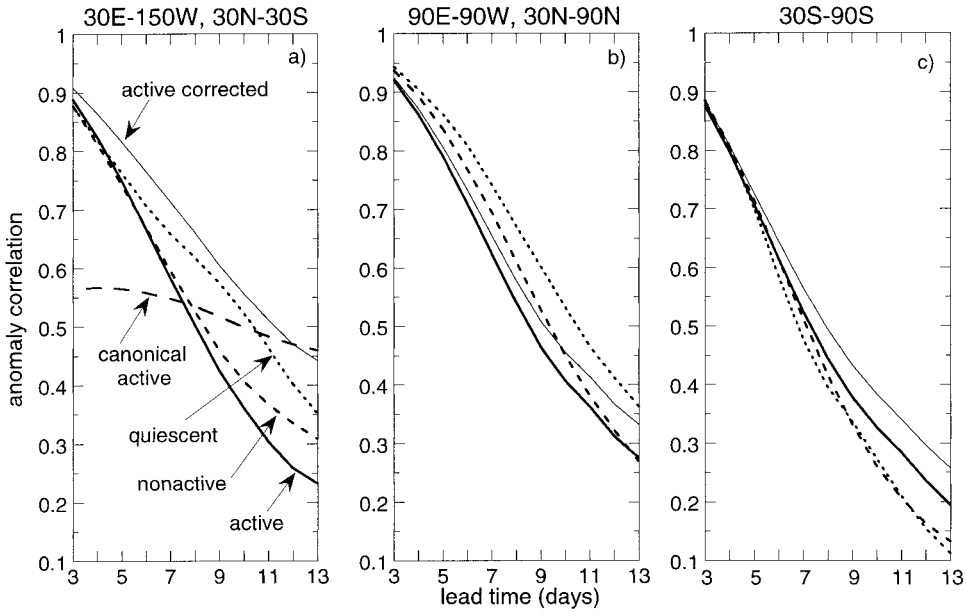

FIG. 12. Anomaly correlations between forecasts, as functions of lead time, and verification of the 200-mb streamfunction for (a) the tropical region 30°N–30°S, 30°E–150°W, (b) the Northern Hemisphere extratropical region 30°–90°N, 90°E–90°W, and (c) the Southern Hemisphere extratropics 30°–90°S. Correlations are shown for all forecasts initialized when the MJO was active and quiescent, as given by the dates in Table 1 and for times when the MJO is nonactive. Empirically corrected anomaly correlations are also shown for the forecasts initialized when the MJO was active (labeled ''active corrected''). Also shown in (a) is the anomaly correlation for the canonical MJO, which is formed by lag regression of the verifying analyses onto the leading two principal components of OLR at the initial forecast time.

has been argued to be appropriate if this model is interpreted as an equivalent barotropic model applied at the 200-mb level (e.g., Borges and Sardeshmukh 1995), although the response is not particularly sensitive to the damping timescale owing to the short integrations reported here. Weak biharmonic diffusion also is included with coefficient 2.34×10^{16} m^4 s^{-1}.

The simulated eddy streamfunction error from the

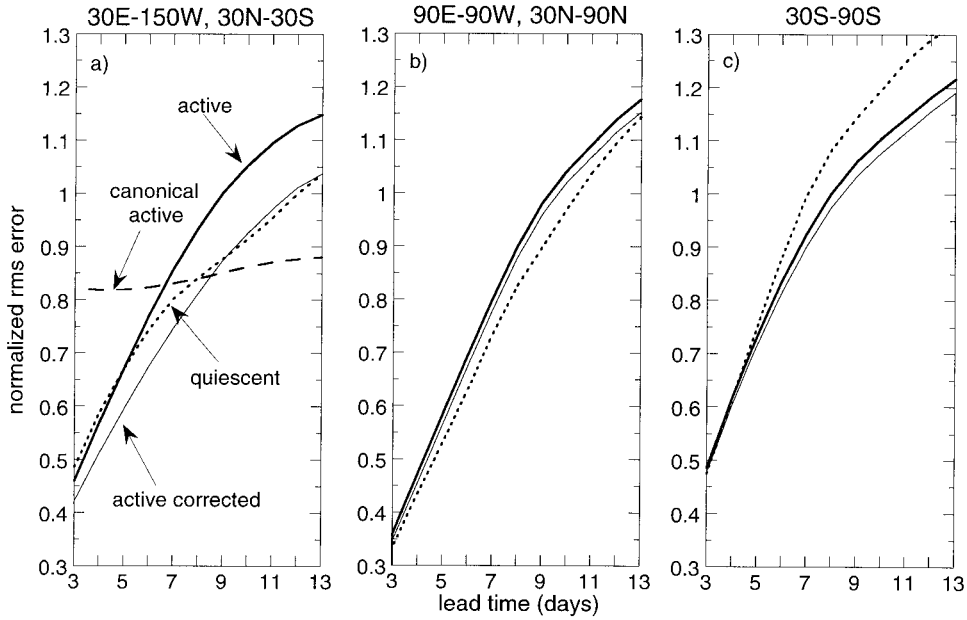

FIG. 13. As in Fig. 12 except for the rms error normalized by the rms of the verification.

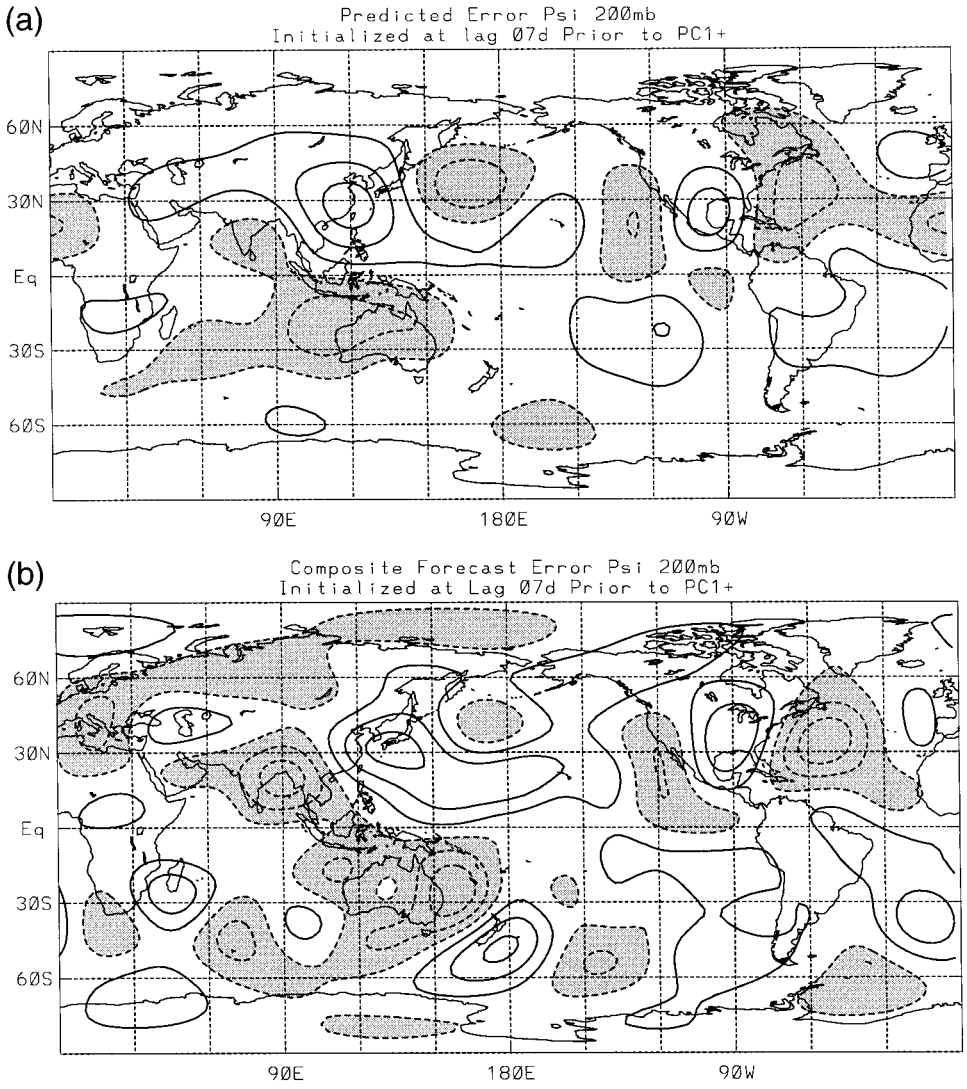

FIG. 14. (a) Simulated and (b) composite 7-day forecast error of the eddy 200-mb streamfunction anomaly for PC1+. The simulated error was computed in the barotropic vorticity model forced by the composite tropical 200-mb divergence error for forecasts initialized 7 days before the maximum of PC1+. Contour interval is 2.5×10^6 m^2 s^{-1} with the first contour at $\pm 1.25 \times 10^6$ m^2 s^{-1}. Negative values are shaded.

barotropic model for the forecasts initialized 7 days prior to the maximum of PC1+ is shown in Fig. 14a. Performance of the barotropic model for reproducing the errors for the other three phases is similar (not shown). The day 7 error is shown because the composite error from the MRF model (Fig. 10b and reproduced again in Fig. 14b) is well established by then. At subsequent times the simulated error by the barotropic model is progressively poorer downstream in the extratropics, due presumably to both the shortcomings of the barotropic model applied at the 200-mb level and neglect of other forcing (e.g., transient eddy vorticity fluxes). Nonetheless, reasonable agreement between the simulated error from the barotropic vorticity model and composite forecast for day 7 is seen. In particular, the erroneous cyclone–anticyclone over the Indian and western Pacific Oceans, associated with the collapse of the MJO-induced convection in the MRF, is well simulated. The errors associated with the extratropical wave trains are essentially reproduced, though systematic zonal contraction and lack of meridional propagation occurs downstream of the forcing in both hemispheres. Considering the simplicity of this barotropic model, the overall agreement is supportive of the hypothesis that global forecast errors associated with the MJO have their root in the failure of the MRF model to sustain the convectively driven, divergent tropical circulation produced by the MJO.

The relative import of tropical divergence forcing and free Rossby wave dispersion from the initial condition upon the extratropical forecasts is further explored by using the barotropic vorticity model to simulate the evo-

TABLE 2. Global anomaly correlations between the 7-day simulation of the 200-mb streamfunction anomalies from the barotropic vorticity model and the composite analyses that verify each of the four phases of the MJO. Correlations are computed for simulations forced with the observed composite 200-mb tropical divergence, the composite of the 200-mb tropical divergence from the 7-day forecasts from the MRF model, and no divergence forcing. The barotropic simulations were initialized with the observed composite streamfunction anomalies 7 days before the maxima of each of the PCs. Correlations listed in parenthesis are for simulations initialized with zero streamfunction anomaly.

	Observed divergence forcing		Forecast divergence forcing		No divergence forcing
PC1+	0.40	(0.38)	0.30	(0.28)	−0.01
PC2+	0.52	(0.65)	0.15	(0.51)	−0.44
PC1−	0.50	(0.58)	0.34	(0.49)	−0.45
PC2−	0.37	(0.32)	0.20	(0.25)	−0.10

lution of the actual anomalous streamfunction (rather than the forecast error) using both observed and forecast divergence forcing. Integrations are begun from observed initial conditions and at-rest initial conditions. Integrations are also performed starting from observed initial conditions but with no forcing. These unforced simulations are in the same vein as Sardeshmukh et al. (1997), who showed that the observed low-frequency evolution of the extratropical circulation cannot be explained by integrating the unforced barotropic vorticity model from observed initial conditions alone.

Results of these runs are summarized in Table 2, which displays global anomaly correlations between the 7-day prediction of anomalous streamfunction from the barotropic vorticity model and the observed composite streamfunction averaged for each of the four phases of the MJO. Correlations for the barotropic simulations starting from observed initial conditions using observed divergence forcing are systematically larger than for the barotropic simulations using the forecast divergence from the MRF. These larger correlations for the observed divergence forcing are consistent with the ability of the barotropic model to simulate the composite streamfunction error given the composite tropical divergence error (Fig. 14). The anomaly correlations using no forcing but observed initial conditions are much smaller and even negative, indicating that the evolution of the intraseasonal circulation anomalies associated with the MJO cannot be viewed simply as free Rossby wave propagation and dispersion from an initial perturbation, even considering the zonal asymmetries of the basic state (see also Sardeshmukh et al. 1997). The importance of the tropical divergence forcing is further underscored by observing that the correlations for the two forced cases (observed and forecast tropical divergence) starting from an at-rest initial condition are similar to those starting from observed initial conditions.

7. Discussion and conclusions

Impact of the tropical MJO on medium-range (3–15 days) predictions was assessed using 5 yr of daily forecasts for November–March from the reanalysis version of the NCEP MRF model. This model was found unable to sustain the eastward propagating, convectively coupled tropical circulation anomalies produced by the MJO when initialized at times the MJO is active. This particular model furthermore is unable to develop an active MJO when initialized prior to such observed development. Systematic errors in the Tropics fully develop by about day 7, by which time the convectively coupled components of the MJO have decayed to zero in the forecast. Extratropical forecast errors, associated with the collapse of the tropical divergence anomalies, fully develop by day 10. These errors initially (i.e., through forecast day 7) are due to Rossby wave trains dispersing from the erroneous tropical divergence.

In the Tropics and Northern Hemisphere extratropics, forecasts initialized prior to or during active episodes of the MJO were found to have systematically less skill at medium range than forecasts initialized when the MJO is quiescent or nonactive (see also Chen et al. 1993). This reduced skill was ascribed to the systematic decay of the tropical circulation and precipitation anomalies associated with the MJO. This result does not imply that the MRF ably forecasts other convectively coupled tropical variability unrelated to the MJO. Rather, the decreased skill results because the MJO is both the dominant mode of variability and covariability of convection and circulation (e.g., Zhang and Hendon 1997). In fact, the level of convective variability during active periods of the MJO is about 20% greater across the Indian and west Pacific Oceans than during inactive periods. Hence, even if the MRF were equally poor at simulating interaction and coupling of convection with circulation at other intraseasonal time- and space scales, forecasts during active episodes of the MJO might be expected to have systematically worse skill because of the dominance of the MJO. Whether the systematic collapse of the MJO results from deficiencies in the model's convective parameterizations, from errors in the initial conditions, or from neglect of ocean–atmosphere coupling is unknown, but is worth reconciling as future forecast improvements may be aided by this knowledge.

This reduction of skill during active episodes of the MJO is in apparent contradiction with Lau and Chang (1992). They claimed that the MJO was more active and that medium-range skill in a similar version of the MRF was better in the second of two 60-day periods beginning on 12 December 1986. Our opinion is that much of the divergence variability captured by the leading EOFs of velocity potential for this period, which they used to estimate MJO activity, is unrelated to the MJO, despite the fact that the leading EOFs have zonal wavenumber 1 structure. Such low wavenumber structure is a consequence of the nonlocal nature of the velocity potential and not necessarily a reflection of divergence with a similar structure (e.g., Hendon 1986). Examination of OLR maps for this period reveals not only

active MJOs,[5] but strong synoptic-scale activity in the monsoon trough and in the South Pacific convergence zone, particularly in the second 60-day period, that projects onto the leading EOF of velocity potential. Thus, while we agree with Lau and Chang that medium-range skill in the Tropics was indeed better in the second 60-day period, we argue that this increase in skill is not a result of demonstrably stronger MJO activity.

We did find that medium-range skill for forecasts initialized during active episodes of the MJO was markedly increased by removal of the systematic model error associated with the MJO. In fact, empirical correction of the forecasts during active episodes of the MJO extends the skill in the Tropics, as measured by when the anomaly correlation drops below 0.5, from 6 to 11 days. However, medium-range skill of the corrected forecasts in the Northern Hemisphere extratropics is extended only by about 1 day. This more modest increase in skill is consistent with the fact that the signal of the MJO in the extratropics is much weaker than in the Tropics.

This empirical correction does not allow for interaction with transient eddies, whose cumulative effects could have potentially larger impacts than direct tropical divergence forcing on extratropical medium-range forecasts (e.g., Cai et al. 1996). By continually relaxing the Tropics to the verification during extended-range forecasts, which does allow for full interaction between the tropically forced extratropical circulation and transient eddies, Ferranti et al. (1990) found a significant increase in extratropical medium-range skill during active episodes of the MJO. Taken together, these results are indicative that medium-range skill in the Tropics and Northern Hemisphere extratropics can be significantly improved during active episodes of the MJO with a proper simulation of intraseasonal convective activity in the Tropics.

Interestingly, in the Southern Hemisphere extratropics medium-range skill was found to be systematically worse during quiescent periods of the MJO, even compared to the skill of uncorrected forecasts during active periods of the MJO. Such a result suggests that initial conditions associated with the MJO may have as pronounced an impact on medium-range forecasts in the Southern Hemisphere extratropics as does a proper simulation of the Tropics, at least during austral summer when the mean stationary waves there are relatively weak.

Acknowledgments. Fruitful discussions with J. Whitaker and insightful comments by H. Van den Dool, C. Zhang, and three anonymous reviewers are gratefully acknowledged.

[5] The dates in Table 1 suggest that the MJO was weaker in the second 60-day period. However, examination of the OLR PCs reveals that an event beginning in late February 1987 (i.e., during Lau and Chang's second 60-day period) just failed to reach our 1.5 sigma criterion. The Hovmöller plot of 200-mb zonal wind for winter 1986/87 in Slingo et al. (1996) also indicates that the MJO was equally active in the second 60-day period.

REFERENCES

Borges, M. D., and P. D. Sardeshmukh, 1995: Barotropic Rossby wave dynamics of zonally varying upper-level flows during northern winter. *J. Atmos. Sci.,* **52,** 3779–3796.

Cai, M., J. S. Whitaker, R. M. Dole, and K. L. Paine, 1996: Dynamics of systematic errors in the NMC medium range forecast model. *Mon. Wea. Rev.,* **124,** 265–276.

Chen, S.-C., J. O. Roads, and J. C. Alpert, 1993: Variability and predictability in an empirically forced global model. *J. Atmos. Sci.,* **50,** 443–463.

Ferranti, L., T. N. Palmer, F. Molteni, and E. Klinker, 1990: Tropical–extratropical interaction associated with the 30–60 day oscillation and its impact on medium and extended range prediction. *J. Atmos. Sci.,* **47,** 2177–2199.

Hendon, H. H., 1986: Streamfunction and velocity potential representation of equatorially trapped waves. *J. Atmos. Sci.,* **43,** 3038–3042.

——, and B. Liebmann, 1990: A composite study of onset of the Australian summer monsoon. *J. Atmos. Sci.,* **47,** 2227–2240.

——, and J. D. Glick, 1997: Intraseasonal air–sea interaction in the tropical Indian and Pacific Oceans. *J. Climate,* **10,** 647–661.

Higgins, R. W., and K. C. Mo, 1997: Persistent North Pacific circulation anomalies and the tropical intraseasonal oscillation. *J. Climate,* **10,** 223–244.

Hsu, H.-H., 1996: Global view of the intraseasonal oscillation during northern winter. *J. Climate,* **9,** 2386–2406.

Kalnay, E., and Coauthors, 1996: The NCEP/NCAR 40-Year Reanalysis Project. *Bull. Amer. Meteor. Soc.,* **77,** 437–471.

Kessler, W. S., M. J. McPhaden, and K. M. Weickmann, 1995: Forcing of intraseasonal Kelvin waves in the equatorial Pacific. *J. Geophys. Res.,* **100,** 10 613–10 631.

Knutson, T. R., and K. M. Weickmann, 1987: 30–60 day atmospheric oscillations: Composite life cycles of convection and circulation anomalies. *Mon. Wea. Rev.,* **115,** 1407–1436.

Lau, K.-M., and T. J. Phillips, 1986: Coherent fluctuations of extratropical geopotential height and tropical convection in intraseasonal timescales. *J. Atmos. Sci.,* **43,** 1164–1181.

——, and F. C. Chang, 1992: Tropical intraseasonal oscillation and its prediction by the NMC operational model. *J. Climate,* **5,** 1365–1378.

Liebmann, B., and C. A. Smith, 1996: Description of a complete (interpolated) outgoing longwave radiation dataset. *Bull. Amer. Meteor. Soc,* **77,** 1275–1277.

——, H. H. Hendon, and J. D. Glick, 1994: The relationship between tropical cyclones of the western Pacific and Indian Oceans and the Madden–Julian oscillation. *J. Meteor. Soc. Japan,* **72,** 401–412.

Lorenc, A. C., 1984: The evolution of planetary-scale 200 mb divergent flow during the FGGE year. *Quart. J. Roy. Meteor. Soc.,* **110,** 427–441.

Nakazawa, T., 1986: Intraseasonal variations of OLR in the Tropics during the FGGE year. *J. Meteor. Soc. Japan,* **64,** 17–34.

Newman, M., P. D. Sardeshmukh, and J. W. Bergman, 2000: An assessment of the NCEP, NASA and ECMWF reanalyses over the tropical west Pacific warm pool. *Bull. Amer. Meteor. Soc.,* in press.

Salby, M. L., and H. H. Hendon, 1994: Intraseasonal behavior of clouds, temperature, and winds in the Tropics. *J. Atmos. Sci.,* **51,** 2207–2224.

Sardeshmukh, P. D., and B. J. Hoskins, 1988: On the generation of global rotational flow by steady idealized tropical divergence. *J. Atmos. Sci.,* **45,** 1228–1251.

——, M. Newman, and M. D. Borges, 1997: Free barotropic Rossby

wave dynamics of the winterime low-frequency flow. *J. Atmos. Sci.,* **54,** 5–23.

Schemm, J. E., H. Van den Dool, and S. Saha, 1996: A multi-year DERF experiment at NCEP. Preprints, *11th Conf. on Numerical Weather Prediction,* Norfolk, VA, Amer. Meteor. Soc., 47–49.

Shinoda, T., H. H. Hendon, and J. D. Glick, 1999: Intraseasonal surface fluxes across the tropical Indian and western Pacific Oceans from NCEP reanalyses. *Mon Wea. Rev.,* **127,** 678–693.

Simmons, A. J., J. Wallace, and G. Branstator, 1983: Barotropic wave propagation and instability and atmospheric teleconnection patterns. *J. Atmos. Sci.,* **40,** 1363–1392.

Slingo, J. M., and Coauthors, 1996: Intraseasonal oscillations in 15 atmospheric general circulation models: Results from an AMIP diagnostic subproject. *Climate Dyn.,* **12,** 325–357.

Wang, B., and X. Xie, 1998: Coupled modes of the warm pool climate system. Part I: The role of air–sea interaction in maintaining Madden–Julian oscillations. *J. Climate,* **11,** 2116–2135.

Zhang, C., 1996: Atmospheric variability at the surface in the western Pacific Ocean. *J. Atmos. Sci.,* **53,** 739–758.

——, and H. H. Hendon, 1997: Propagating and standing components of the intraseasonal oscillation in tropical convection. *J. Atmos. Sci.,* **54,** 741–752.